SANDIA REPORT

SAND97-1205 • UC-401
Unlimited Release
Printed June 1997

An Implicit Fast Fourier Transform Method for Integration of the Time Dependent Schrodinger or Diffusion Equation

A. Burke Ritchie, Merle E. Riley

Prepared by
Sandia National Laboratories
Albuquerque, New Mexico 87185 and Livermore, California 94550

Sandia is a multiprogram laboratory operated by Sandia Corporation, a Lockheed Martin Company, for the United States Department of Energy under Contract DE-AC04-94AL85000.

Approved for public release; distribution is unlimited.

Sandia National Laboratories

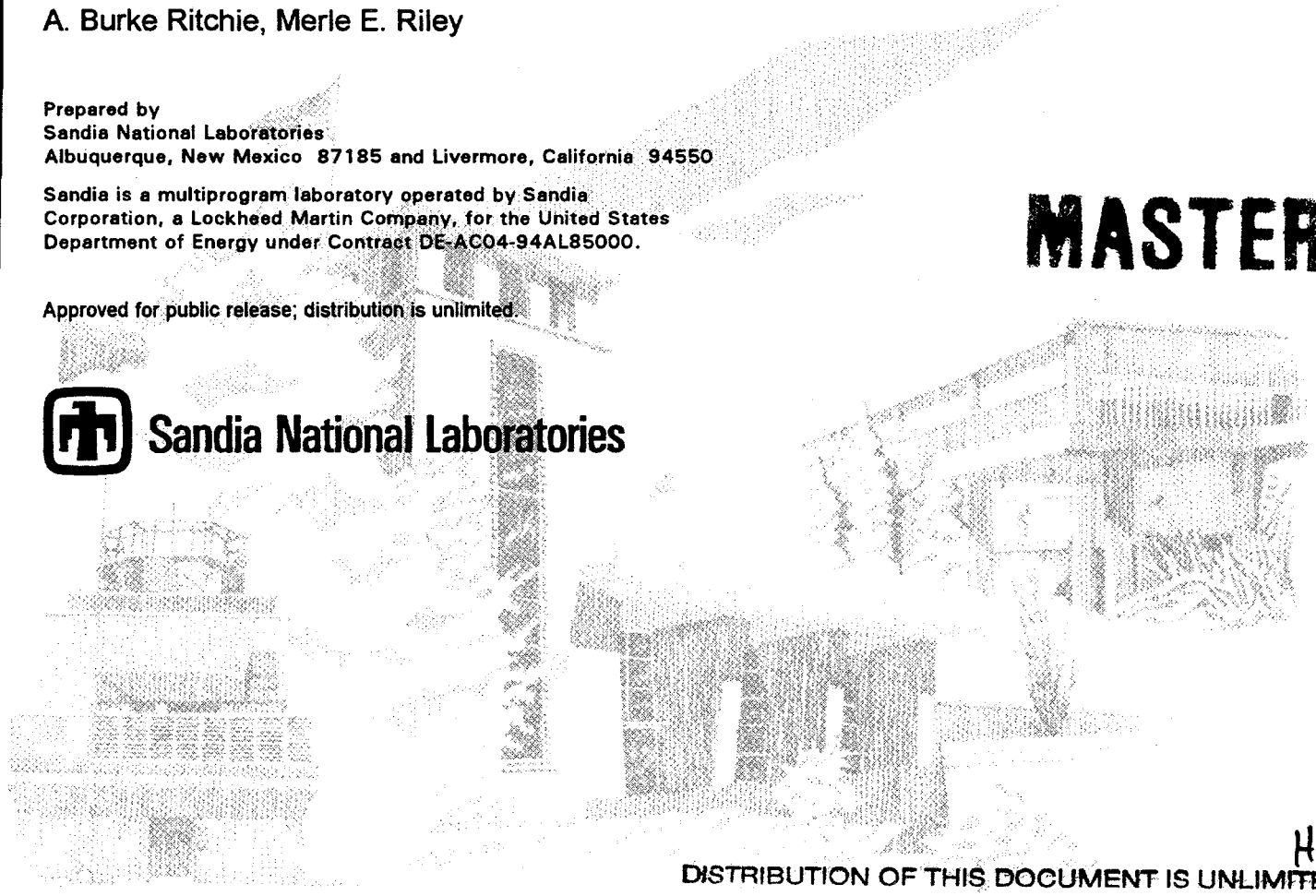

Issued by Sandia National Laboratories, operated for the United States Department of Energy by Sandia Corporation.

Available to DOE and DOE contractors from
Office of Scientific and Technical Information
P.O. Box 62
Oak Ridge, TN 37831

Prices available from (615) 576-8401, FTS 626-8401

Available to the public from
National Technical Information Service
U.S. Department of Commerce
5285 Port Royal Rd
Springfield, VA 22161

NTIS price codes
Printed copy: A03
Microfiche copy: A01

DISCLAIMER

SAND97-1205
Unlimited Release
Printed June 1997

Distribution
Category UC-401

An Implicit Fast Fourier Transform Method for Integration of the Time Dependent Schrodinger or Diffusion Equation

A. Burke Ritchie
Lawrence Livermore National Laboratory
Livermore, CA 94550
and
Merle E. Riley
Laser, Optics, and Remote Sensing Department
Sandia National Laboratories
P.O. Box 5800
Albuquerque, NM 87185-1423

Abstract

We have found that the conventional exponentiated split operator procedure is subject to difficulties in energy conservation when solving the time-dependent Schrodinger equation for Coulombic systems. By rearranging the kinetic and potential energy terms in the temporal propagator of the finite difference equations, one can find a propagation algorithm for three dimensions that looks much like the Crank-Nicholson and alternating direction implicit methods for one- and two-space-dimensional partial differential equations. We report comparisons of this novel implicit split operator procedure with the conventional exponentiated split operator procedure on hydrogen atom solutions. The results look promising for a purely numerical approach to certain electron quantum mechanical problems.

I. Introduction

The potential of the new massively-parallel-processor computers to perform "bare-knuckle" numerical solutions of difficult full-dimensional problems prompted us to investigate some modern finite-difference methods for solution of partial differential equations of interest, among these the time-dependent Schrodinger equation (TDSE). There are several choice methods for integration of the TDSE.[1] One of the more interesting is the exponentiated split operator procedure (ESOP),[1,2] based on the use of the fast Fourier transform (FFT), which has been successfully used for vibration-rotation spectral analysis and simple scattering situations.[1,3,4] In fact the ESOP with FFT is widely used in both optical and quantum physics for wave propagation. These previous successes suggest an investigation of the ESOP and FFT for novel atomic physics situations.

Electronic processes such as charge transfer, excitation, and ionization involve the Coulomb interaction which makes the numerical representation of the wave function more difficult than in the molecular dynamics studies.[2,3,4] We have found that the ESOP tends to be very sensitive to the integration step size in Coulombic problems: the solutions become inaccurate very abruptly as the time increment is increased. Overall, one would prefer a method with the inherent stability of implicit numerical procedures which, although inaccurate for large step sizes, remain stable and acceptable in overall character. In this introduction we review the ESOP and introduce a novel numerical method, the implicit split operator procedure (ISOP), which is reminiscent of the Crank-Nicolson (CN) and alternating-direction implicit (ADI) methods[5] for integrating the TDSE or diffusion equation. It is hoped that this new finite difference algorithm for solving the TDSE and related problems will make the massively-parallel-processor computers more useful for problems in atomic and molecular physics.

The TDSE is written as

$$\dot{\Psi} = -i H \Psi \tag{1}$$

in Hartree atomic units (denoted au), which will be used throughout this report. The Hamiltonian is:

$$H = T + V,$$
$$T = -\tfrac{1}{2}\nabla^2. \qquad (2)$$

The potential V is a function of position and possibly time. The ESOP formulates the numerical integration as the repeated application of the factored (split) incremental propagator:

$$\Psi_{t+dt} = \exp(-\tfrac{1}{2}iT\,dt)\,\exp(-iV\,dt)\,\exp(-\tfrac{1}{2}iT\,dt)\,\Psi_t. \qquad (3)$$

The reasoning for this numerical form has been discussed[1,2] previously. Basically, by using the speed of the FFT to convert from the space to momentum representation and back, one can always apply *diagonal* operators to the wave function. We should add here that the ESOP conserves norm but not energy due to the lack of commutation of the incremental propagator with the Hamiltonian. The procedure is correct through order $(dt)^2$ and the truncation error is proportional to commutators of T and V operating on the initial wave function. This immediately suggests that the ESOP is to be preferred for situations where the potential is smooth compared to the wave function. In these cases the truncation error should remain small even for large time steps.

In certain atomic physics applications we found that the truncation error in the ESOP grew faster than we could tolerate with time steps that would have appeared to be adequate for a second-order-accurate method. The energy $\langle\Psi|H|\Psi\rangle / \langle\Psi|\Psi\rangle$ was an immediate symptom of the error growth. These were applications with a Coulomb potential and a hydrogen 1s orbital as a part of the wave function. In order to improve upon the solution to such a problem, we recalled that the implicit CN method would be a good start for a one-space-dimensional problem. Generalizations to two space dimensions in the form of the ADI method are practical, but three space dimensional solutions are tentative at best.[5] We begin by writing down the second-order-accurate, time-symmetric form of the finite difference advance in the TDSE, analogous to the CN procedure:

$$\Psi_{t+dt} + \tfrac{1}{2}iH\,dt\,\Psi_{t+dt} = \Psi_t - \tfrac{1}{2}iH\,dt\,\Psi_t. \qquad (4)$$

A direct numerical solution of Eq.(4) is impractical due to the difficulties in resolving the implicit part of the operator, even with the use of ADI techniques. The truncation error in Eq.(4) is $O(dt)^3$, which is precisely the same as in the ESOP in Eq.(3). What is desired is a use of the fast Fourier transform (FFT) methods for resolving Eq.(4) by splitting the space and momentum parts of the Hamiltonian. One way to do this is to rewrite Eq.(4):

$$\Psi_{t+dt} = \frac{1-\frac{1}{2}iH\,dt}{1+\frac{1}{2}iH\,dt}\Psi_t \tag{5}$$

and to factor the propagator quotient *approximately*, all the while *maintaining* accuracy through $O(dt)^2$ precisely as in Eq.(3):

$$\Psi_{t+dt} = \left(\frac{1-\frac{1}{4}iT\,dt}{1+\frac{1}{4}iT\,dt}\right)\left(\frac{1-\frac{1}{2}iV\,dt}{1+\frac{1}{2}iV\,dt}\right)\left(\frac{1-\frac{1}{4}iT\,dt}{1+\frac{1}{4}iT\,dt}\right)\Psi_t\,. \tag{6}$$

The advantage of this factorization or splitting is that the operator is now a product of momentum and coordinate dependencies which allows the FFT procedure to be applied as in the ESOP. We refer to the form in Eq.(6) as the implicit split operator procedure (ISOP). Other factorizations may be better - we do not have any prescription at the moment for choosing a unique form of the factored propagator. If one is willing to drop the requirement of second-order accuracy, *fully* implicit factorizations are feasible which may be more suitable for certain other applications.[6]

II. Numerical Study of Stationary State

Our numerical study compares calculations on the hydrogen atom with the two methods, ESOP and ISOP. First we explore stability of the stationary, time-independent 1s state with the propagators. In Table I for the ESOP we tabulate the results for a set of spatial volumes, given as the cube of the box side, and a set of time step increments. The FFT was chosen to be a $(64)^3$ grid. The time solution went from zero to 200 au. The grid was centered symmetrically about the Coulomb singularity. An investigation of a non-centered grid with a cutoff (r = max[$r, 0.13au$]) imposed on V=$-1/r$ gave similar results (see Appendix). In all cases the space points were element centered and quadratures were performed by the trapezoidal rule.

L^3 (au^3)	dt (au)	H(0) (au)	H(200) (au)	comments
$(10)^3$	0.02	-0.49462	-0.48241	
"	0.05	"	+4.97	bad
$(20)^3$	0.05	-0.47931	-0.47941	
"	0.1	"	+2.58	bad (Fig.1 & 2)
$(40)^3$	0.05	-0.43196	-0.43200	
"	0.1	"	-0.43209	
"	0.2	"	-0.43245	
"	0.5	"	+4.97	bad

Table I. ESOP study of the isolated H atom propagated over 200 au in time for differing box sizes and time steps. The FFT grid is 64 points in each of x, y, and z. H(0) and H(200) denote the energy at the beginning and end of the computation.

In Table I we note the appearance of a "Courant-like" condition in the fact that a larger space increment allows stable integration with a larger time step. Of course the error is not good for the use of a grid much sparser than the $(64)^3$ grid in a (40 au)^3 box about the H 1s orbital where the resultant space increment is about 0.6 au. Fig. 1 shows the dramatic growth of the error in energy as a function of time. The error is in the kinetic energy, as may be seen in the noisy part of the wave function that is growing in the large-r region outside the main 1s orbital in Fig. 2. This error tends to be rapidly varying in space and thus it dominates the kinetic energy term of the Hamiltonian.

An analogous set of calculations on H using the ISOP gave the results in Table II. We note that larger step sizes may now be used with reasonable resulting energies.

L^3 (au^3)	dt (au)	H(0) (au)	H(200) (au)	comments
$(10)^3$	0.05	-0.49462	-0.49339	
"	0.1	"	-0.48441	
"	0.2	"	-0.46591	
"	0.5	"	-0.45502	smooth error
$(20)^3$	0.05	-0.47931	-0.47945	
"	0.1	"	-0.47931	
"	0.2	"	-0.47493	
"	0.5	"	-0.45490	(Fig. 3 & 4)
$(40)^3$	0.05	-0.43196	-0.43198	
"	0.1	"	-0.43203	
"	0.2	"	-0.43216	
"	0.5	"	-0.42691	

Table II. ISOP study of the H atom propagated over 200 au in time for differing box sizes and time steps. The FFT grid is 64 points in each of x, y, and z. H(0) and H(200) denote the energy at the beginning and end of the computation.

The error that develops in the ISOP is different - it tends to remain smooth and thus has a small effect on the kinetic energy. In Fig. 3 we show the time dependence of the ISOP quantities for one of the runs of Table II. The variations in kinetic and potential energy tend to be somewhat larger than the total energy, but one must remember that the time step is *ten times as large* as the largest stable time step found for the ESOP method for the cases in Table I. The ISOP error is evident as smooth undulations in the extreme wings of the wave function plotted in Fig. 4.

III. Numerical Study of Time-Evolving State

Here we wish to examine the evolution of a time-dependent problem with some dynamic content. We again pick the H atom but now with a "kicked" or impulsively excited state at time zero. The initial wave function is

$$\Psi = \phi_{1s} \exp(i k_o z) = \frac{1}{\sqrt{\pi}} e^{-r} \, e^{i k_o z} \,, \qquad (7)$$

where we have chosen $k_o = 0.25$ for these numerical solutions. We have also selected the L = 20 au box and the $(64)^3$ grid with time integration form 0 to 200 au. Because the impulsively excited state has a significant amplitude in the H atom continuum, we must allow for electron probability to be lost from our numerical "boxed" system. We do this by Kulander's procedure[7] of covering the interior of the box with an imaginary optical potential which is several grid points in thickness. We found that a value of the optical potential (γ, in reciprocal time units) of 0.2 performed quite well.

In Figs. 5 and 6 we show the results of ISOP with a time increment of 0.025 au. An analogous ESOP run gives nearly identical results. At the end of the run, the electron mean positions agree to within 4%, the lost probability is 0.042 for both runs, and the energies are both -0.4732 au. These results are believed to be accurate solutions for the given box and absorptive optical potential. In Figs.7 and 8 we show the ESOP results for a time step of 0.2 au. The energy is bad and the wave function is being lost much too rapidly from the box because of the amplitude of the noisy part of the wave function in the region of the optical potential. In Table I we found that an ESOP step of 0.1 was inadequate for the stationary H atom in this box and grid. For the time-dependent problem here, though, a step of 0.1 is only marginally bad because the optical potential acts to damp the erroneous, noisy part of the amplitude. This gives a fortuitous cancellation of errors and makes the ESOP run look better than it should. An examination of the wave function for this case in Fig. 8 reveals a persistent component of the noisy amplitude in the continuum like that seen in Fig. 2.

In Fig. 9 we demonstrate the ISOP performance with a larger time step of 0.5 au. The final wave function is shown in Fig. 10. The probability decrease is 0.058, which is large, but the norm is nearly constant as to be contrasted with the ESOP solution. The major error is the oscillation in position which grows out of phase as may be seen by comparing to the converged runs in Fig. 5. Again we have demonstrated stable performance of the ISOP with a time step which is an order of magnitude larger than the ESOP.

In computations that are not shown here, we have done limited charge exchange calculations of protons on H at lab energies of 1, 4, and 100 keV at impact parameters of 1, 3, and 5 au. Qualitatively, the results look as they should for this multichannel rearrangement scattering problem.

IV. Discussion and Conclusion

Within the scope of this study the stability of the ISOP is clearly superior to the ESOP for Coulombic problems. The main feature is a maintenance of stability in the energy conservation as the time increment is increased. This allows the ISOP to perform reasonably with time steps which are an order of magnitude larger than those of the conventional method.

A fundamental question is why the ISOP has any advantage at all over the ESOP. Neither method is energy conservative and both are second-order accurate. We feel that the advantage in the ISOP is due to be Cayley transform representation[8] of the factors in the incremental split propagator. The Cayley transform on a variable X, for example,

$$P_{ISOP} = \frac{1-\frac{1}{2}iX}{1+\frac{1}{2}iX}\,, \qquad (7)$$

as present in the factors of the ISOP propagator, should be compared to the exponentiated equivalent in the ESOP,

$$P_{ESOP} = \exp(-iX)\,. \qquad (8)$$

Both the forms in Eq.(7) and (8) are of modulus unity, but the sizes of the gradients or derivatives are quite different. Consider X to be the Coulomb potential, $X = -1/r$. Examine a component of the gradient, say the x component, operating on the above transforms. The modulus of dP_{ISOP}/dx is bounded as r approaches zero whereas the modulus of dP_{ESOP}/dx diverges. Because the errors in the propagators are proportional to commutators of T and V, which contain derivatives, we feel that this is a rationalization of the advantages of the ISOP.

To conclude, we feel that the improved stability and energy conservation of the ISOP affords direct numerical approaches to the solution of certain quantum mechanical problems. Some of these problems are: strong-field excitation and ionization, charge exchange, multichannel reactive scattering, and wave packet dynamics. The new massively parallel computers can make such approaches practical.

Appendix

A uniformly spaced cartesian grid with points centered about the Coulomb singularity defines its own cutoff of the potential. However one can see that an arbitrarily positioned gridwork can create a large error in the numerical representation of the potential operator if a grid point lies too near the singular point. We make the following argument for the modification of the Coulomb field when used with the FFT grids. Consider the integral over a spherical volume of radius R centered about the singular point of the potential:

$$\int d^3r\, 1/r = 4\pi \int_0^R r^2\, dr\, 1/r = 2\pi R^2 \qquad \text{(A1)}$$

If we equate the spherical volume to the volume of a rectilinear cartesian volume element assuming that the increments are similar in x, y, and z, we find:

$$\begin{aligned} &\tfrac{4}{3}\pi R^3 = (dx)^3, \\ &R = dx\,(3/4\pi)^{1/3}. \end{aligned} \qquad \text{(A2)}$$

If we now equate the integral over the singularity in Eq. (A1) to the trapezoidal value of that integral with a cutoff of r_x imposed in the Coulomb potential , we have

$$2\pi R^2 = (1/r_x)\,(dx)^3, \qquad \text{(A3)}$$

from which we can now solve for r_x using the value of R from Eq.(A2):

$$r_x = (2/9\pi)^{1/3}\, dx \approx 0.414\, dx. \qquad \text{(A4)}$$

The Coulomb potential is simply evaluated with $r = \max[r, r_x]$) . The value of dx in Eq.(A4) is the spatial grid increment, of course. One notes that r_x is less than half of the space increment so that the cutoff is immaterial for grids centered symmetrically about the singularity.

Acknowledgments

We wish to thank Charles Cerjan and Mike Feit for useful information and discussions regarding this work. This work was performed under the auspices of the U. S. Department of Energy by Lawrence Livermore National Laboratory under Contract No. W-7405-ENG-48 and was also supported by the United States Department of Energy under Contract DE-AC04-94AL85000 at Sandia National Laboratores. Sandia is a multiprogram laboratory operated by Sandia Corporation, a Lockheed Martin Company, for the United States Department of Energy.

References:

1. C. Leforestier, R. H. Bisseling, C. Cerjan, M. D. Feit, R. Friesner, A. Guldberg, A. Hammerich, G. Jolicard, W. Karrlein, H.-D. Meyer, N. Lipkin, O. Roncero, and R. Kosloff, "A Comparison of Different Propagation Schemes for the Time Dependent Schrodinger Equation," J. Comput. Phys., 94, 59-80 (1991).

2. M. D. Feit, J. A. Fleck, Jr., and A. Steiger, J. Comput. Phys., "Solution of the Schrodinger Equation by a Spectral Method," 47, 412-433 (1982).

3. M. D. Feit and J. A. Fleck, Jr., "Wave packet dynamics and chaos in the Henon-Heiles system," J. Chem. Phys., 80, 2578-2584 (1984).

4. M. D. Feit and J. A. Fleck, Jr., "Solution of the Schrodinger equation by a spectral method II: vibrational energy levels of triatomic molecules," J. Chem. Phys., 301-308 (1983).

5. W. H. Press, B. P. Flannery, S. A. Teukolsky, and W. T. Vetterling, "Numerical Recipes- The Art of Scientific Computing," Camb. Univ. Press, Camb. and NY (1989).

6. B. Ritchie, P. Dykema, and D. Braddy, "Use of Fast Fourier Transform Computational Methods in Radiation Transport," submitted to Phys. Rev. E, April, 1997.

7. K. C. Kulander, "Multiphoton ionization of hydrogen: A time-dependent theory," Phys. Rev. A, 35, 445-447 (1987).

8. R. G. Newton, "Scattering Theory of Waves and Particles," McGraw Hill Book Co., New York (1966), Ch. 7.

Figure Captions

Figure 1. ESOP on isolated (unperturbed) H 1s orbital with a box of $L^3 = (20\ au)^3$, a FFT grid of $(64)^3$, time integration from 0 to 200 au, and a time step of 0.1 au. The top pane shows the kinetic (dotted), the potential (dashed), and the total energy (solid), all in au. The center pane shows the expectations of the positions, all of which are zero in this case. The lower pane shows the normalization of the wave function as a function of time in au. To be noted is the lack of energy conservation driven by numerical error in the kinetic energy term of the Hamiltonian. These results correspond to the noted case in Table I.

Figure 2. View of the wave function at the end of the computation shown in Fig. 1. The modulus of a two dimensional (x and z) slice of the orbital with $y \approx 0$ is plotted. The numerical noise in the wave function is apparent. These results correspond to the noted case in Table I.

Figure 3. ISOP on isolated (unperturbed) H 1s orbital with a box of $L^3 = (20\ au)^3$, a FFT grid of $(64)^3$, time integration from 0 to 200 au, and a time step of 0.5 au. The plotted quantities are the same as described in Fig. 1. To be noted is the conservation of total energy as compared to Fig. 1, even with a time step that is five times larger. The errors in the individual kinetic and potential energies are more obvious here due to the plot scale. Such ringing errors are a result of the initial orbital not being a precise solution of the finite difference Hamiltonian. These results correspond to the noted case in Table II.

Figure 4. View of the wave function at the end of the computation shown in Fig. 3. The modulus of a two dimensional (x and z) slice of the orbital with $y \approx 0$ is plotted. A careful examination of the figure reveals the smooth type of error present in the ISOP. These results correspond to the noted case in Table II.

Figure 5. ISOP on perturbed H 1s orbital with a box of $L^3 = (20\ au)^3$, a FFT grid of $(64)^3$, time integration from 0 to 200 au, a wavenumber kick of $k_O = 0.25$, and a time step of 0.025 au. The top pane shows the kinetic energy (dotted), the potential energy (dashed), and the total (solid), all in au. The center pane shows the expectations of the positions, with the only non-zero one being $\langle \Psi | z | \Psi \rangle / \langle \Psi | \Psi \rangle$. The lower pane shows the normalization of the wave function as a function of the time. This is a standard

run for comparison with the following figures. Either ISOP or ESOP would give these results to graphical accuracy. To be noted is the loss of normalization (ionization out of kicked state), and apparent stabilization after 100 au of integration time.

Figure 6. View of the wave function at the end of the computation shown in Fig. 5. The modulus of a two dimensional (x and z) slice of the orbital with $y \approx 0$ is plotted.

Figure 7. ESOP on perturbed H 1s orbital with a box of $L^3 = (20 \text{ au})^3$, a FFT grid of $(64)^3$, time integration from 0 to 200 au, a wavenumber kick of $k_o = 0.25$, and a time step of 0.2 au. The plotted quantities are the same as described in Fig. 1. This is an example of an unacceptable numerical solution, which would require ESOP to be run at time steps of 0.1 au or less in order to obtain a useful solution.

Figure 8. View of the wave function at the end of the computation shown in Fig. 7. The modulus of a two dimensional (x and z) slice of the orbital with $y \approx 0$ is plotted. The noise in the wave function is of the same high frequency type as seen in Fig. 2.

Figure 9. Same conditions as Fig. 5 (the standard) except that the ISOP time step has been increased to 0.5 au. Plotted quantities are the same as described in Fig. 1. The ISOP error shows as inaccuracy in phase and amplitude of the electron oscillation.

Figure 10. View of the wave function at the end of the computation shown in Fig. 9. The modulus of a two dimensional (x and z) slice of the orbital with $y \approx 0$ is plotted.. The wave function is quite acceptable even at this large time step.

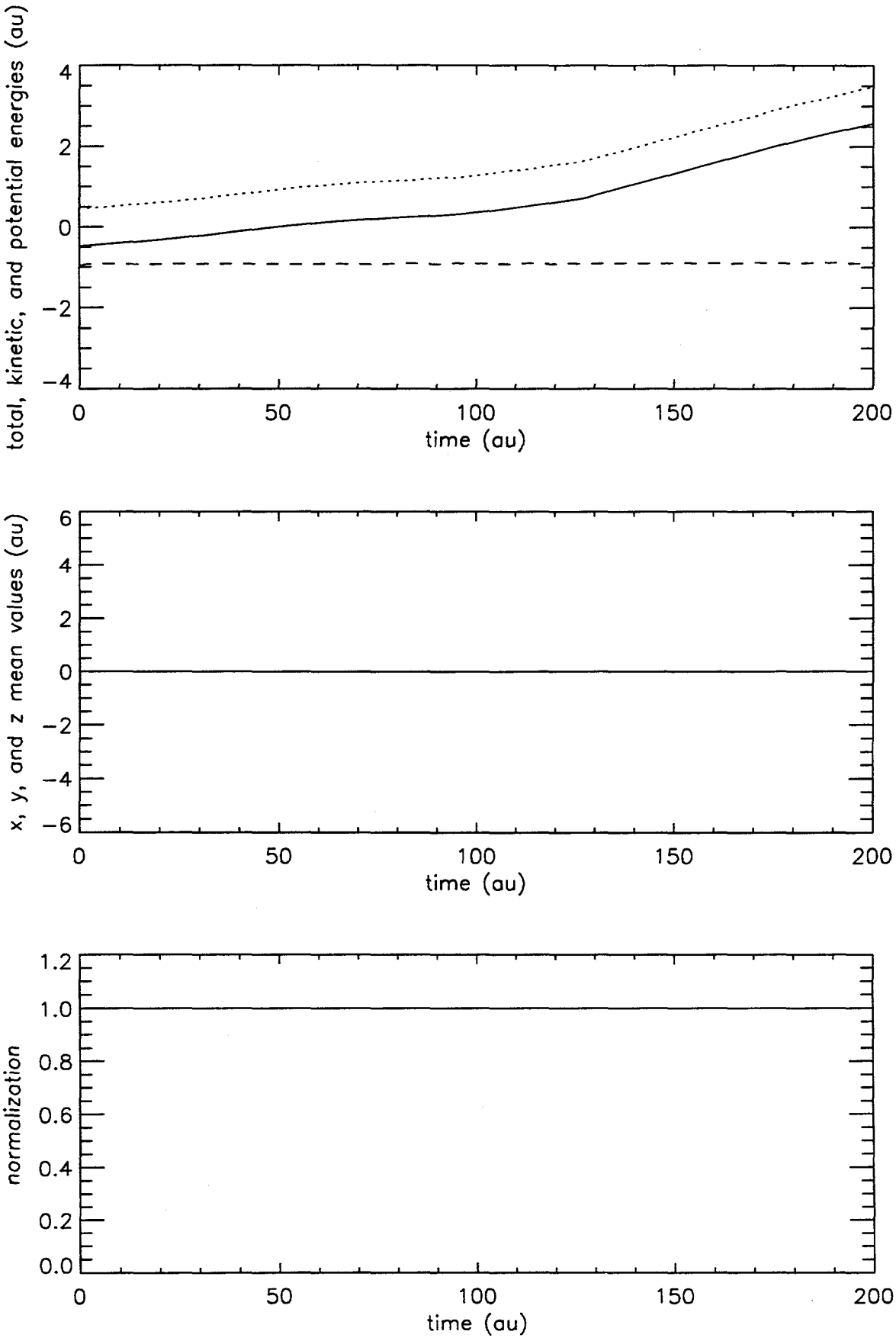
total, kinetic, and potential energies (au)
4
2
0
−2
−4
0
50
100
150
200
time (au)
x, y, and z mean values (au)
6
4
2
0
−2
−4
−6
0
50
100
150
200
time (au)
normalization
1.2
1.0
0.8
0.6
0.4
0.2
0.0
0
50
100
150
200
time (au)

Figure 1

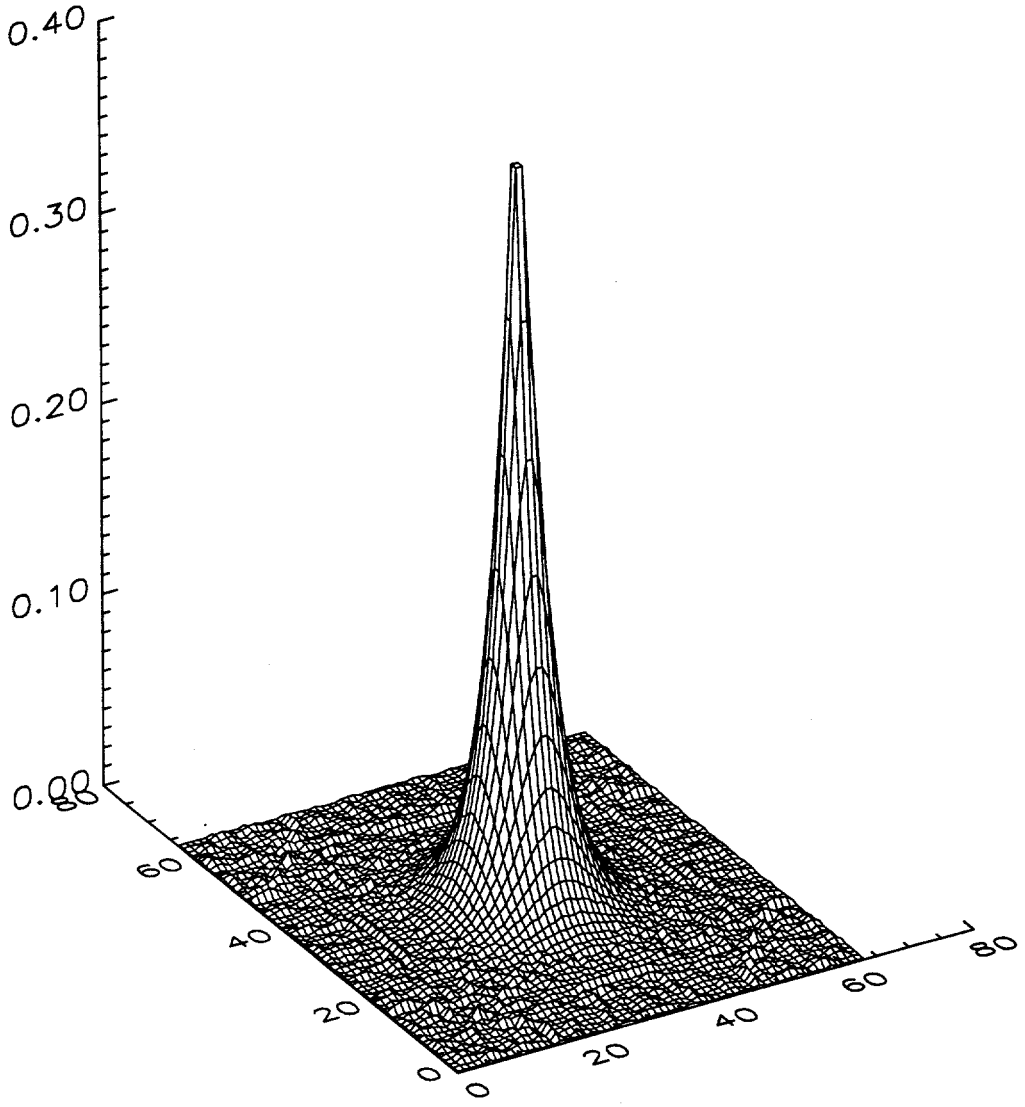

Figure 2

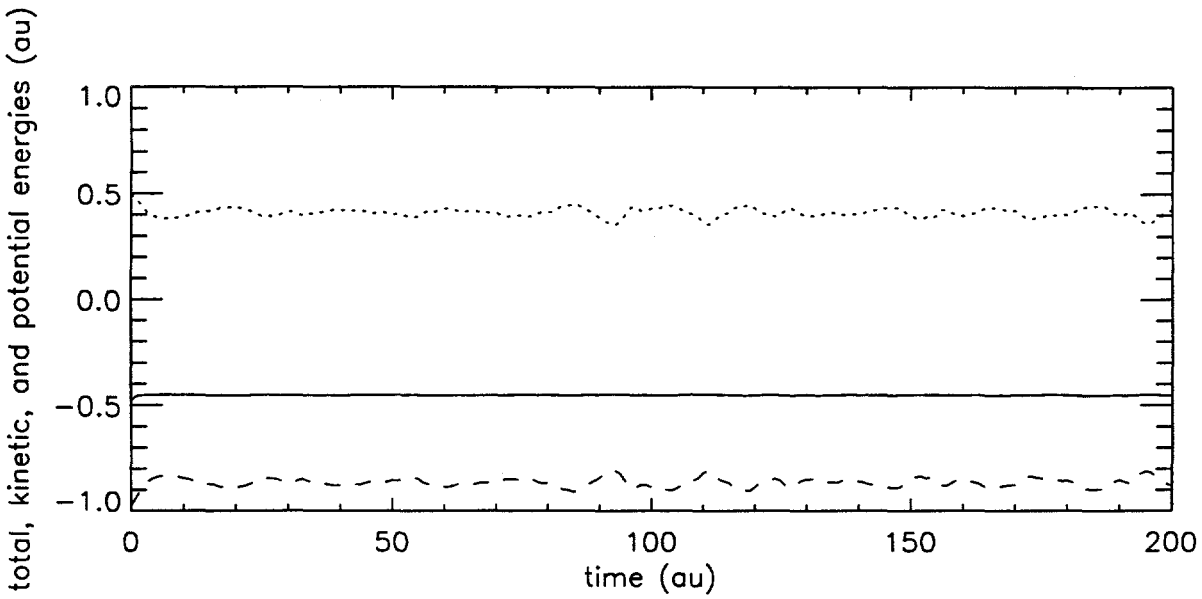
total, kinetic, and potential energies (au)
1.0
0.5
0.0
−0.5
−1.0
0
50
100
150
200
time (au)

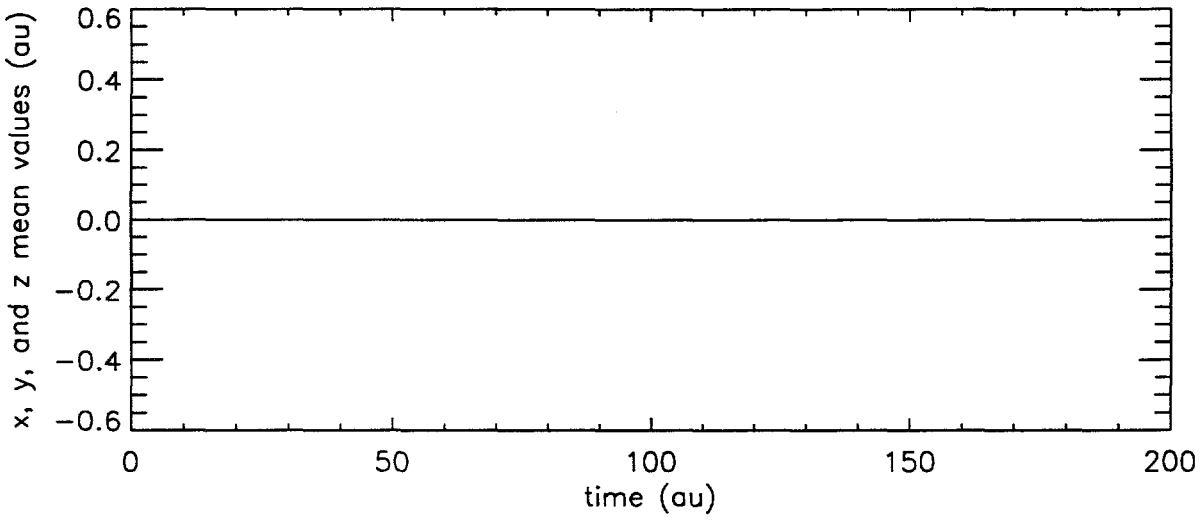
x, y, and z mean values (au)
0.6
0.4
0.2
0.0
−0.2
−0.4
−0.6
0
50
100
150
200
time (au)

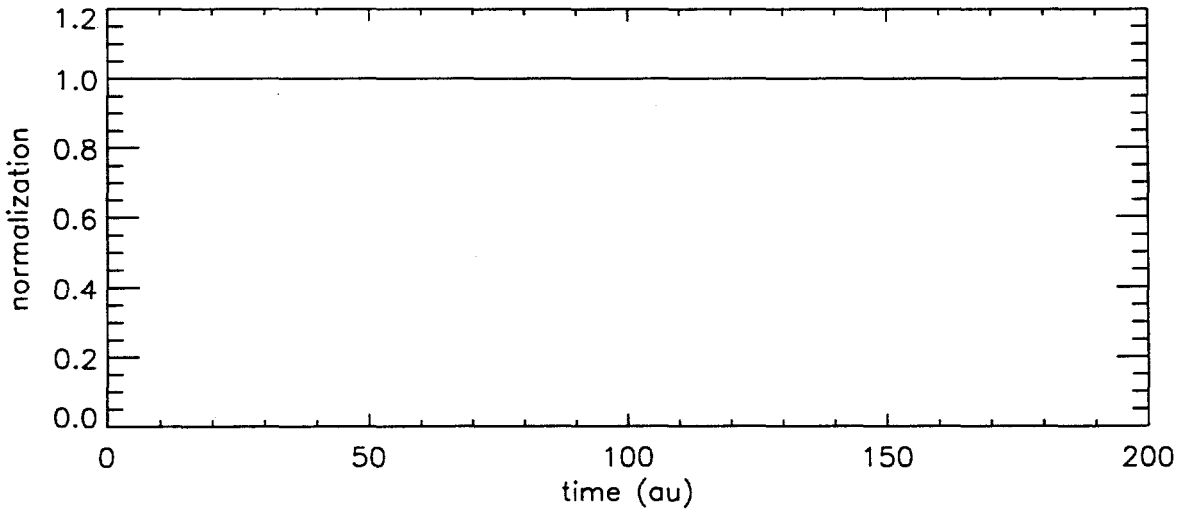
normalization
1.2
1.0
0.8
0.6
0.4
0.2
0.0
0
50
100
150
200
time (au)

Figure 3

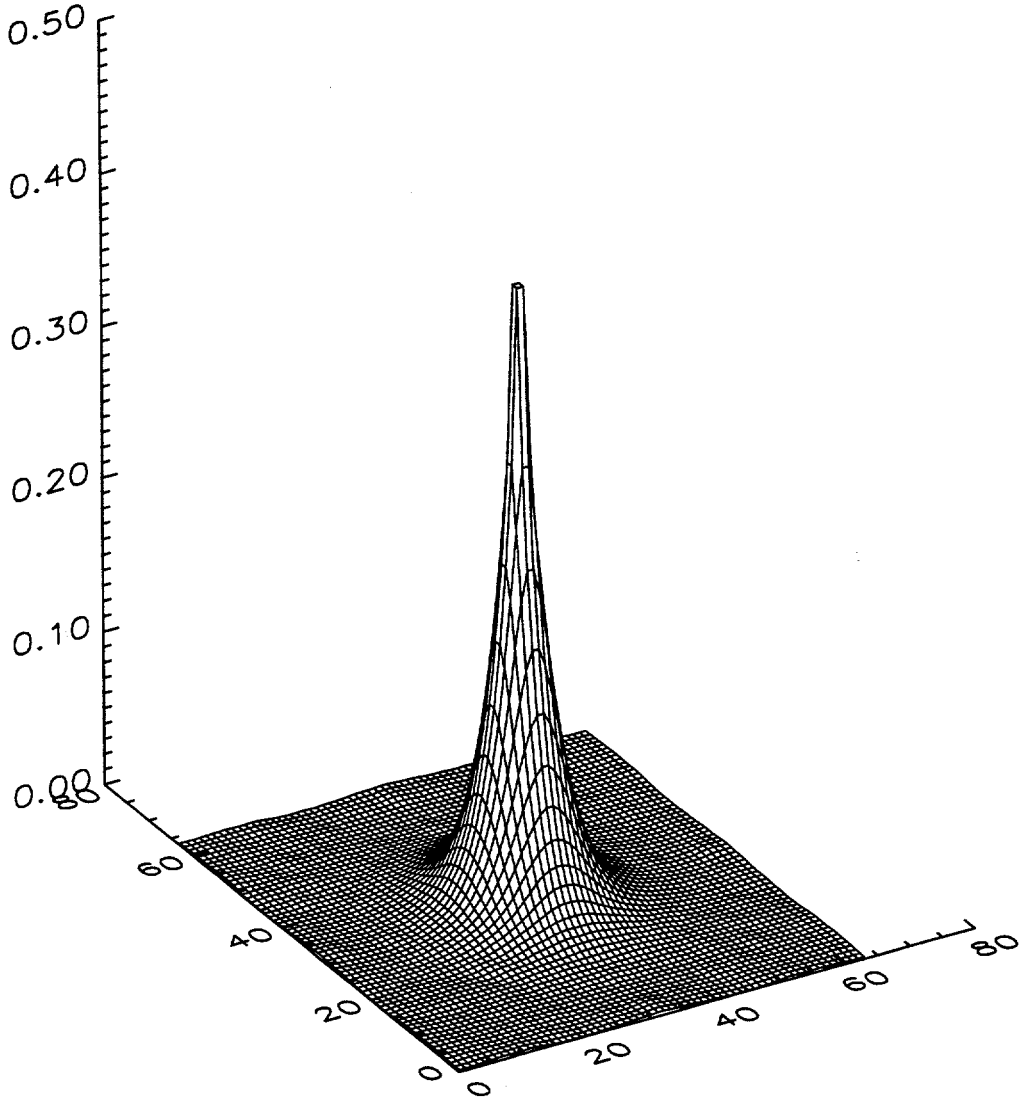

Figure 4

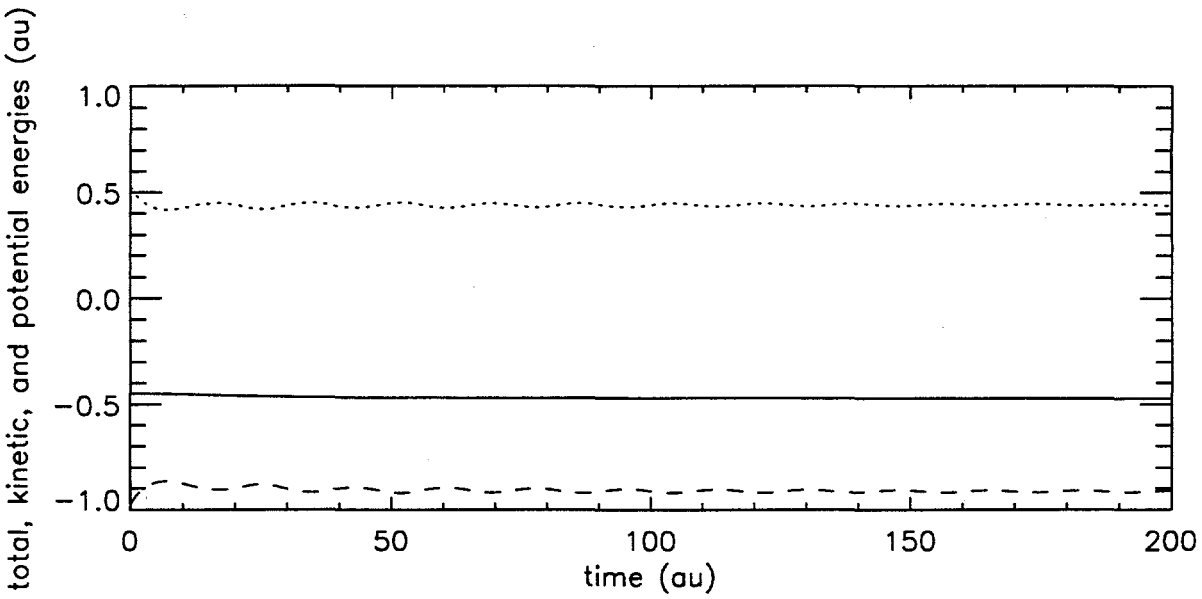
total, kinetic, and potential energies (au)
1.0
0.5
0.0
−0.5
−1.0
0
50
100
150
200
time (au)

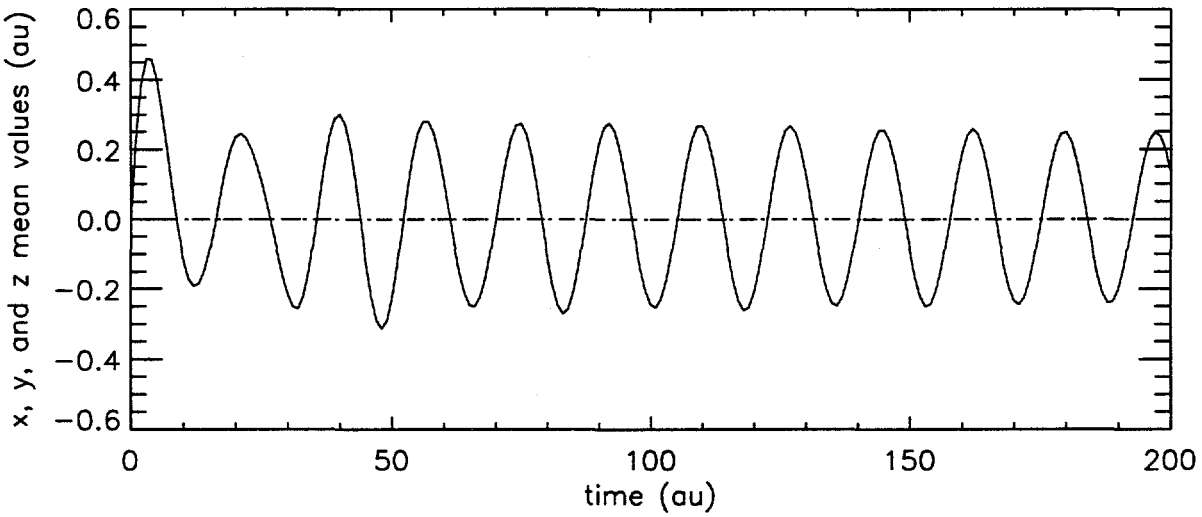
x, y, and z mean values (au)
0.6
0.4
0.2
0.0
−0.2
−0.4
−0.6
0
50
100
150
200
time (au)

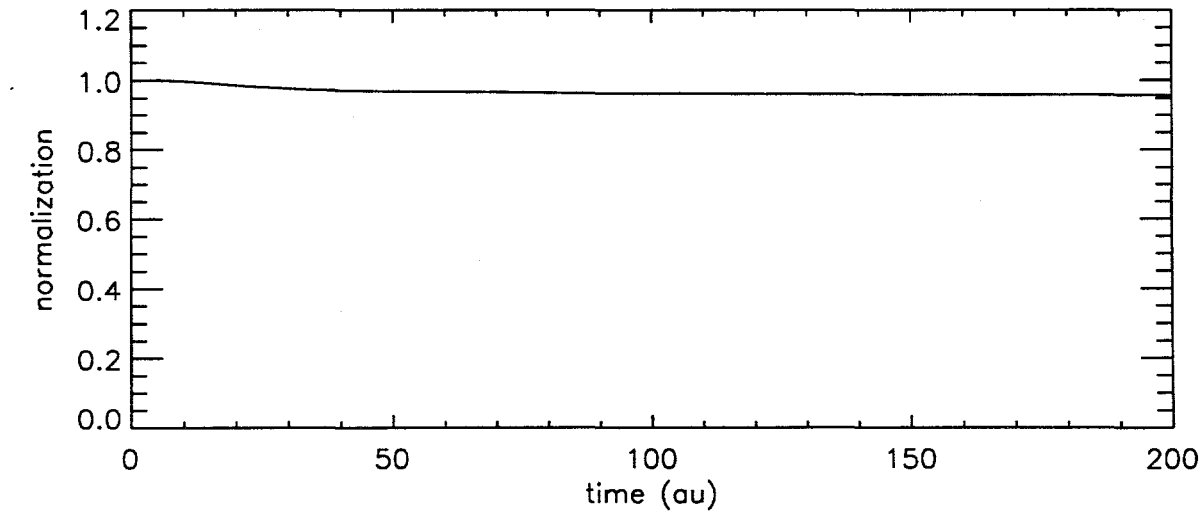
normalization
1.2
1.0
0.8
0.6
0.4
0.2
0.0
0
50
100
150
200
time (au)

Figure 5

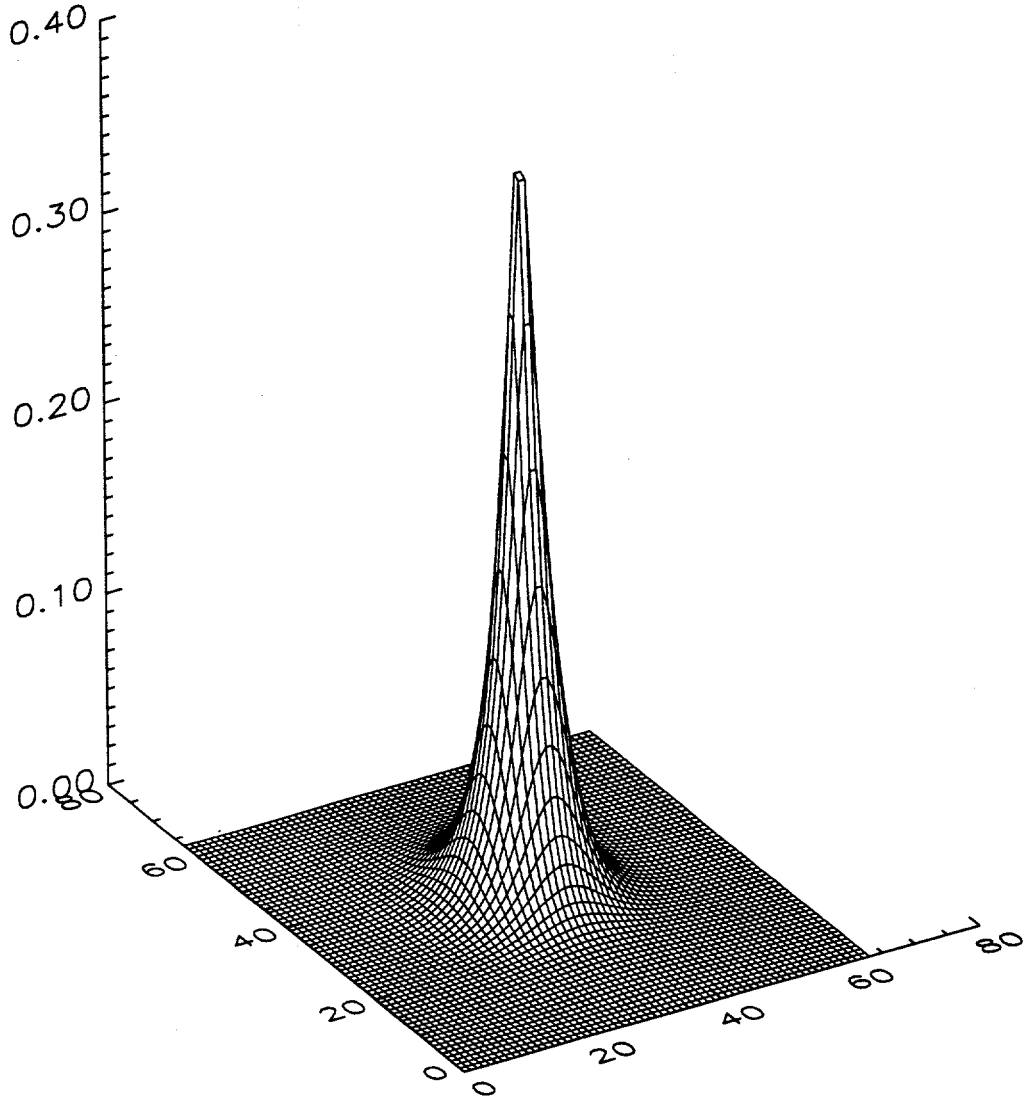

Figure 6

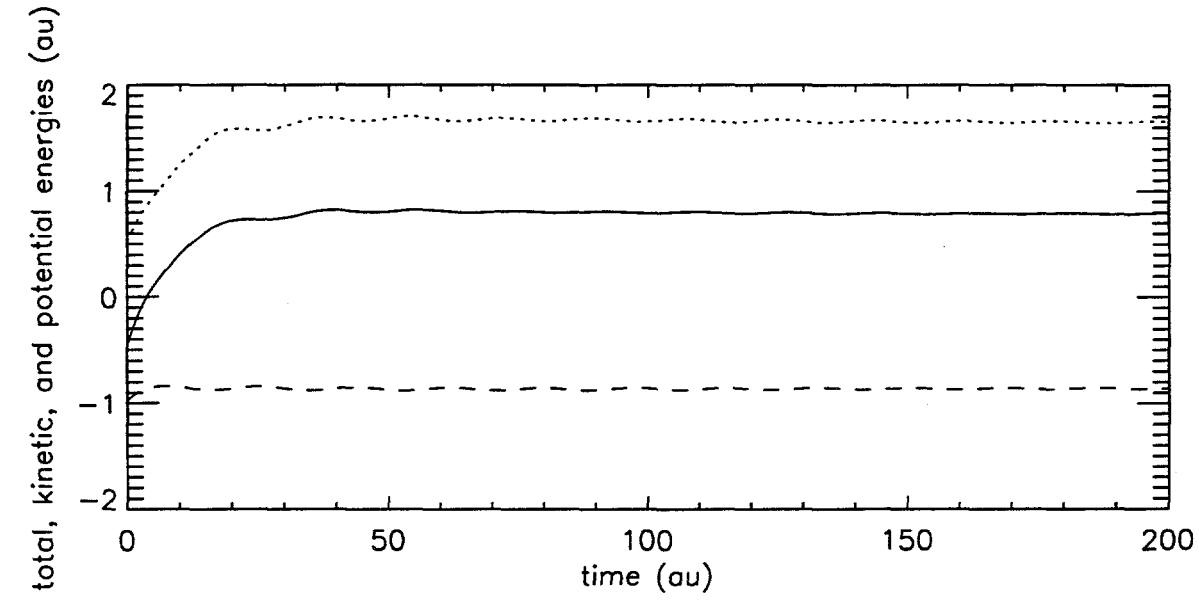
total, kinetic, and potential energies (au)
2
1
0
−1
−2
0
50
100
150
200
time (au)

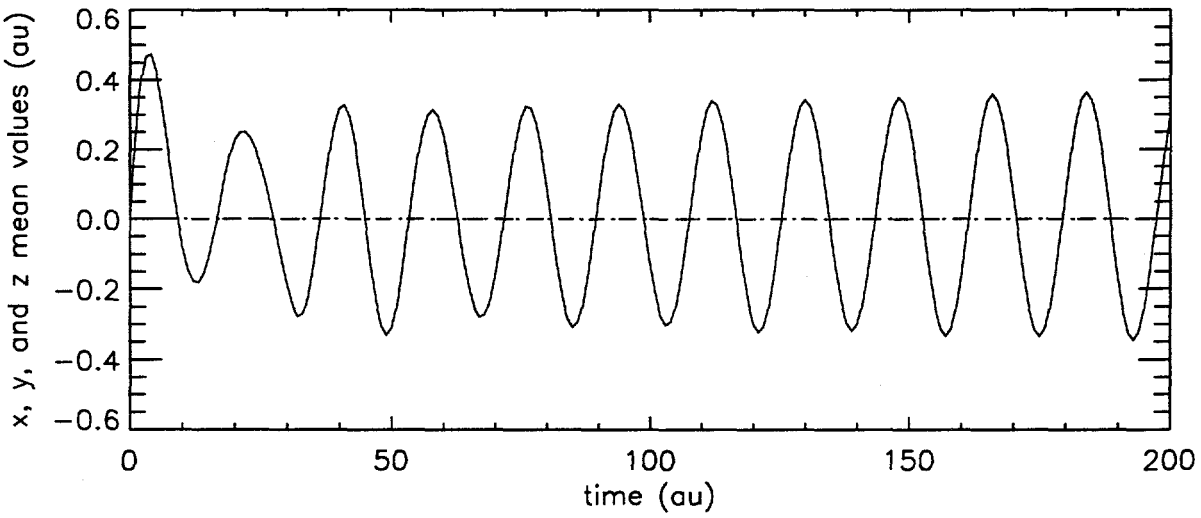
x, y, and z mean values (au)
0.6
0.4
0.2
0.0
−0.2
−0.4
−0.6
0
50
100
150
200
time (au)

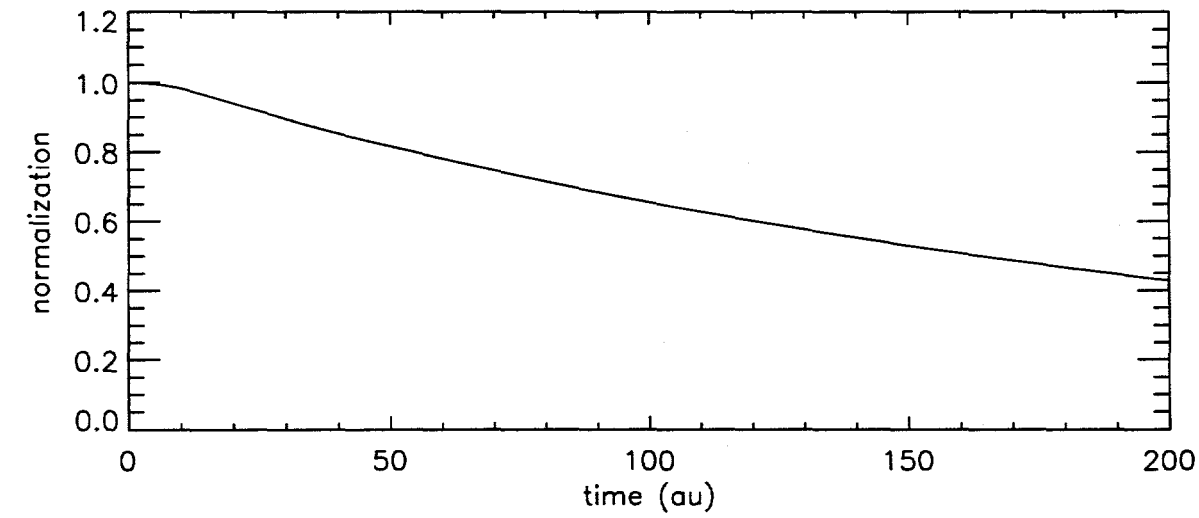
normalization
1.2
1.0
0.8
0.6
0.4
0.2
0.0
0
50
100
150
200
time (au)

Figure 7

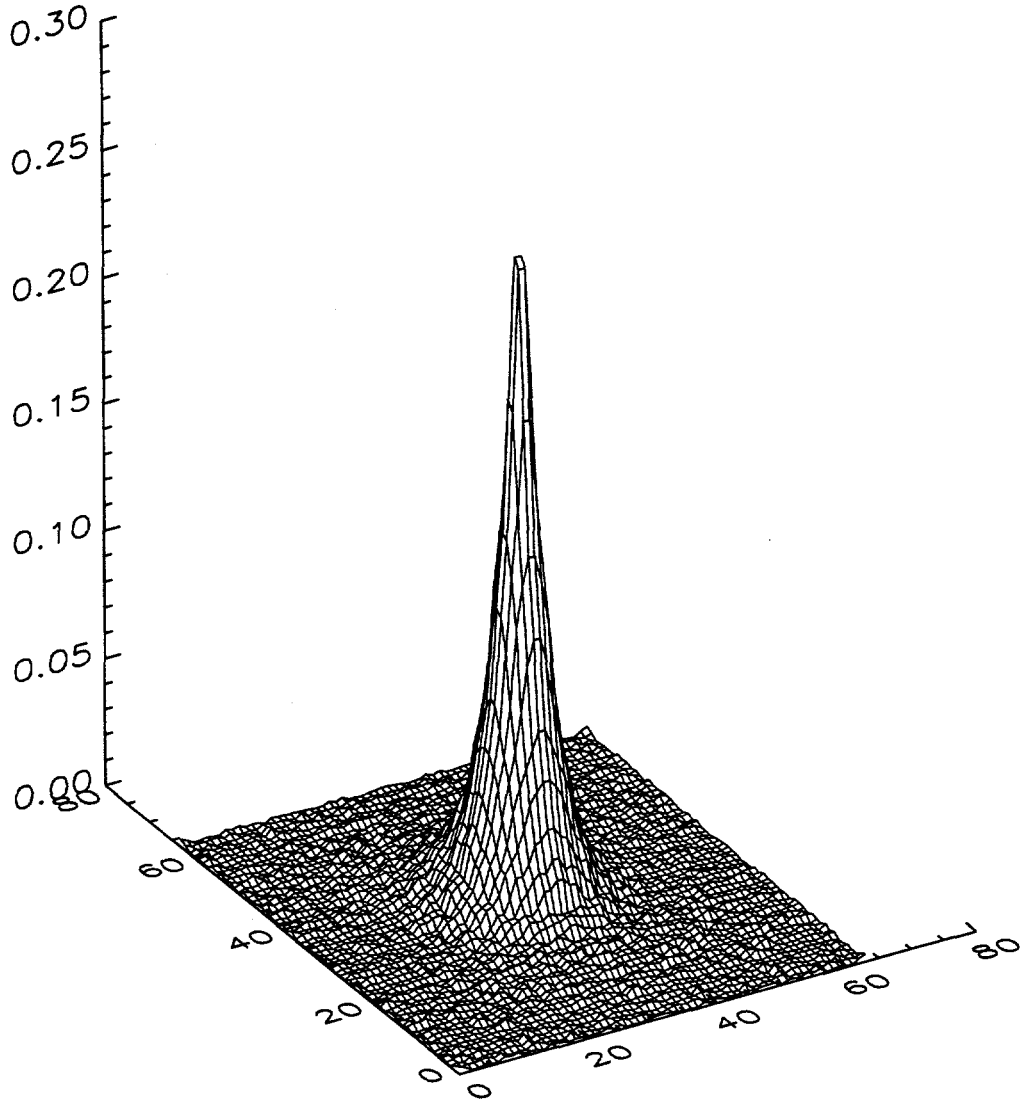

Figure 8

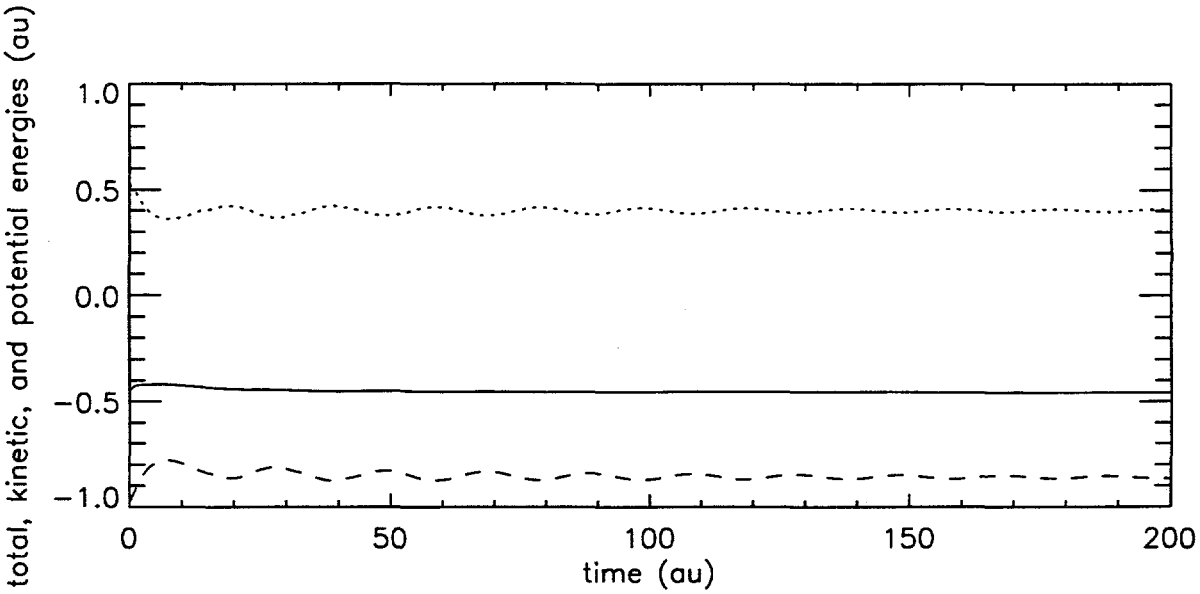
total, kinetic, and potential energies (au)
1.0
0.5
0.0
−0.5
−1.0
0
50
100
150
200
time (au)

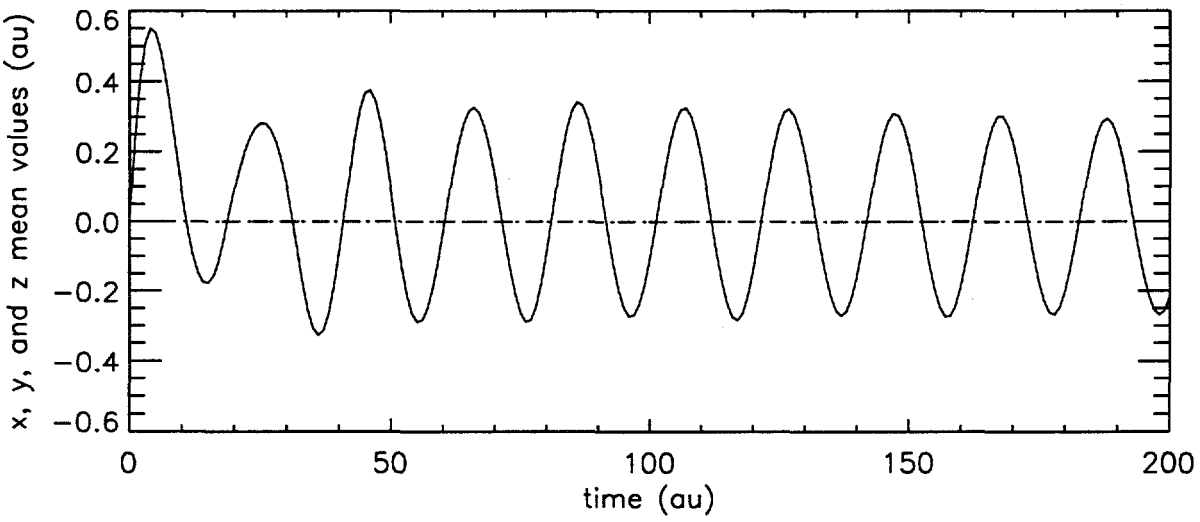
x, y, and z mean values (au)
0.6
0.4
0.2
0.0
−0.2
−0.4
−0.6
0
50
100
150
200
time (au)

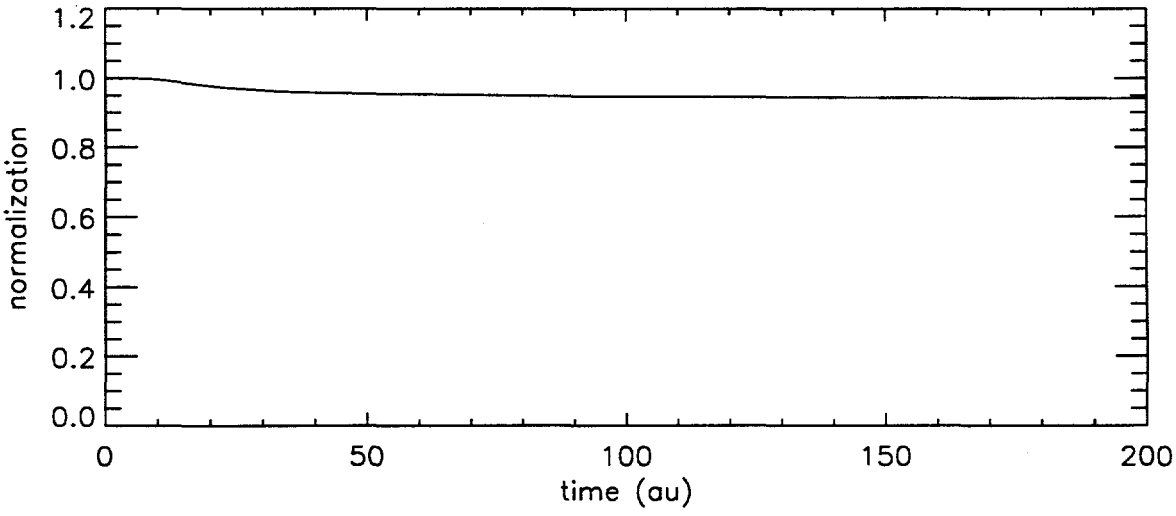
normalization
1.2
1.0
0.8
0.6
0.4
0.2
0.0
0
50
100
150
200
time (au)

Figure 9

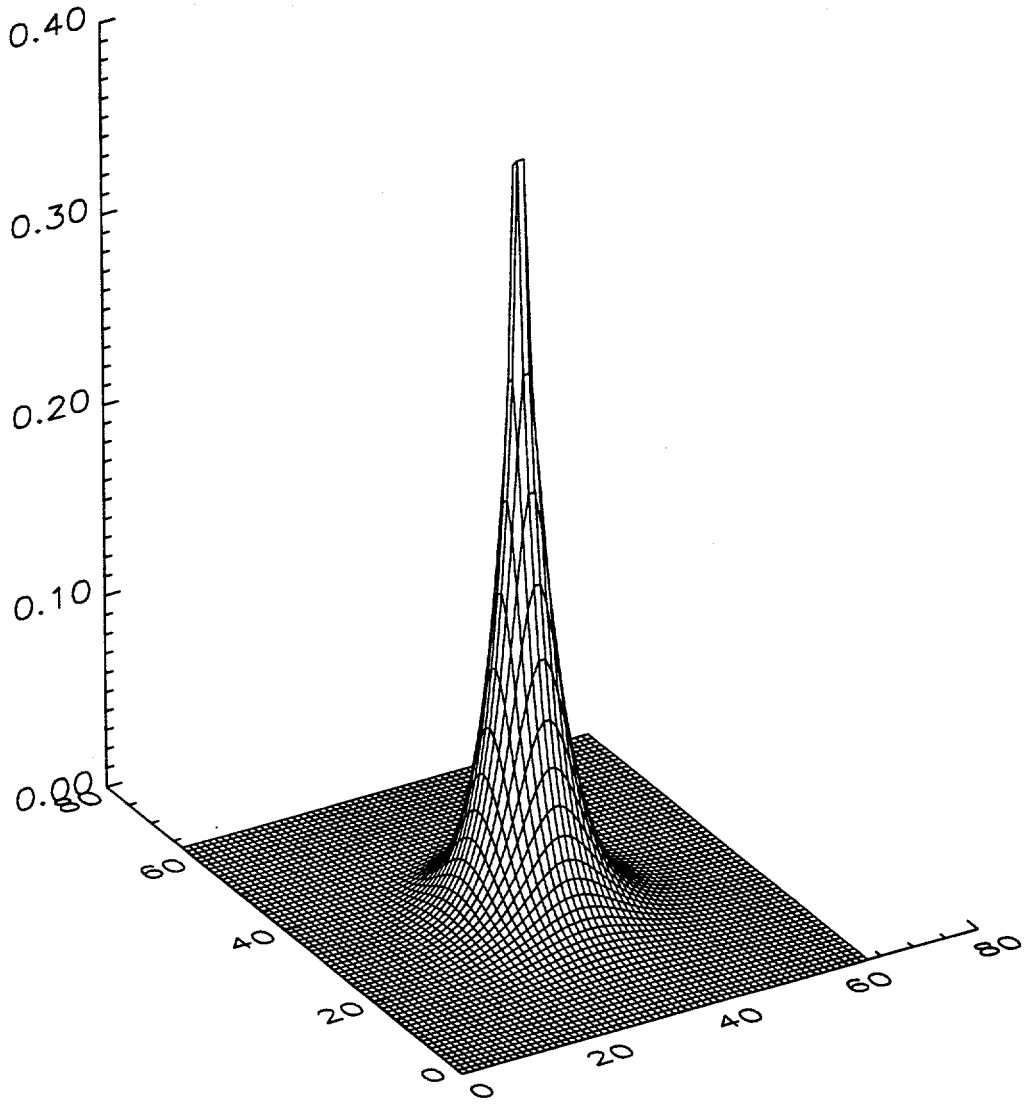

Figure 10

DISTRIBUTION:

1 Lee Collins
T4 B212
Los Alamos National Laboratory
Los Alamos, NM 94550

1 Professor J. Haus
Physics Department
Renssalaer Polytechnic Institute
Troy, NY 12181

1 Professor R. Kosloff
Department of Physical Chemistry
The Hebrew University
Jerusalem 91904, Israel

1 Professor Uzi Landman
School of Physics
Georgia Institute of Technology
Atlanta, GA 30332

1 Professor Michael Pindzola
Physics Department
Auburn University
Auburn, AL 36849

30 Burke Ritchie
L-015 Applied Physics
Lawrence Livermore National Laboratory
Livermore, CA 94550

1 Professor Donald Truhlar
Department of Chemistry
University of Minnesota
Minneapolis, MN 55455

1	MS 0321	W. J. Camp, 9200
1	MS 0827	R. B. Campbell, 9114
1	MS 1111	S. Hutchinson, 9221
1	MS 1111	P. Schultz, 9225
1	MS 1111	M. Sears, 9225
1	MS 1421	E. B. Stechel, 1153
15	MS 1423	M. E. Riley, 1128
1	MS 9018	Central Technical Files, 8940-2
5	MS 0899	Technical Library, 4916
2	MS 0619	Review and Approval Desk, 12690 [For DOE/OSTI]